ONERA ACTIVITIES ON DRAG REDUCTION

J.J. Thibert, J. Reneaux, V. Schmitt
Office National d'Etudes et de Recherches Aérospatiales
Châtillon, France

Abstract

ONERA has been involved for several years in research aiming at transport aircraft drag reduction. This paper presents the main results obtained with the application of some new technologies.

Theoretical design and experimental data of a horizontal tail for an executive aircraft and of a wing for a short haul aircraft are presented for natural laminar flow concept. Much research has also been devoted to hybrid laminar flow control with the studies of a wing, a fin and nacelles for a large transport aircraft.

Expected drag reductions with natural laminar flow and hybrid laminar flow control technologies over conventional turbulent designs are given.

Activities on turbulent skin friction drag have mainly been devoted to the riblets. Tests on a large aircraft model have been carried out in transonic flow in the ONERA S1MA wind tunnel and the results show significant drag reductions.

For other drag components, the paper gives some information concerning the use of a wing tip turbine to reduce the lift-induced drag and the use of the passive shock boundary layer control concept to reduce the wave drag.

1. Introduction.

ONERA's transport aircraft activity represents about twenty per cent of the total activity and involves various areas including aerodynamics, propulsion, structure, materials, flight mechanics and systems.

Concerning aerodynamics, basic or applied research oriented towards medium or long term projects, as well as technical assistance to industry, constitute the main activities.

Taking into account the objectives of the transport aircraft manufacturers, ONERA has been involved these past years in research aiming at transport aircraft drag reduction. This research was carried out in close cooperation by ONERA, manufacturers (Aérospatiale, AMD-BA) and the government agencies (DGAC, STPA).

By looking at a typical transport aircraft drag breakdown like the one shown in Figure 1, it is clear that the main components are the friction drag and the lift induced drag. This is why specific research on these topics has been initiated and in the following sections the main results obtained up to now will be presented.

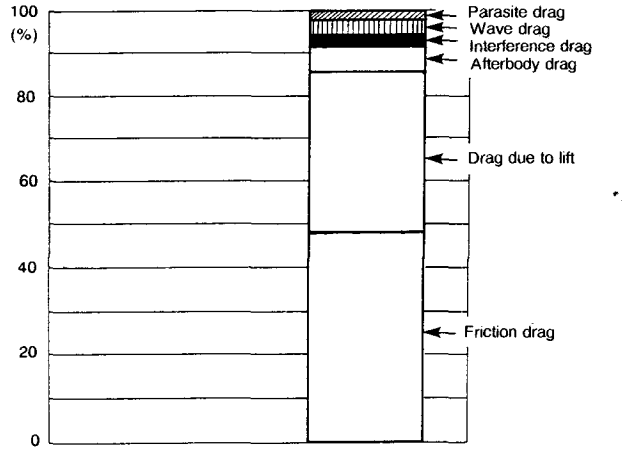

Fig. 1. Aircraft drag breakdown.

2. Skin friction drag reduction

Two methods are generally considered for skin friction drag reduction. The first one aims at delaying the transition on the wing or other components of the aircraft (horizontal tail, fin, nacelles), while the second one aims at reducing the turbulent skin friction.

2.1. Laminar flows

On a swept wing, different types of instabilities may cause transition depending on the sweep angle, the Reynolds number and the pressure gradient. These are shown in Figure 2:

- Tollmien-Schlichting instabilities (TSI);
- crossflow instabilities (CFI);
- attachment line transition (ALT).

For configurations with low or moderate Reynolds numbers, the main causes of transition are laminar separation and streamwise instabilities. For a higher Reynolds number, transition is caused by crossflow instabilities and attachment line transition.

It has long been known that by careful design of the airfoil shape, it is possible to prevent the growth of the Tollmien-Schlichting instabilities and to obtain a large part of laminar flow. However, when increasing the Reynolds number, the negative pressure gradient needed to maintain a laminar flow becomes higher and with the sweep angle this leads to the development of crossflow instabilities. This means that laminarization through the wing shaping (Natural Laminar Flow)[1, 2] could only be applied to the following configurations:

- low sweep and moderate Reynolds number;
- high sweep and small Reynolds number.

For high sweep and high Reynolds number encountered on a large transport aircraft, it is necessary to maintain laminar flow by sucking up the boundary layer on the overall surfaces (Laminar Flow Control[3]) or near the leading edge only (Hybrid Laminar Flow Control[4, 5]).

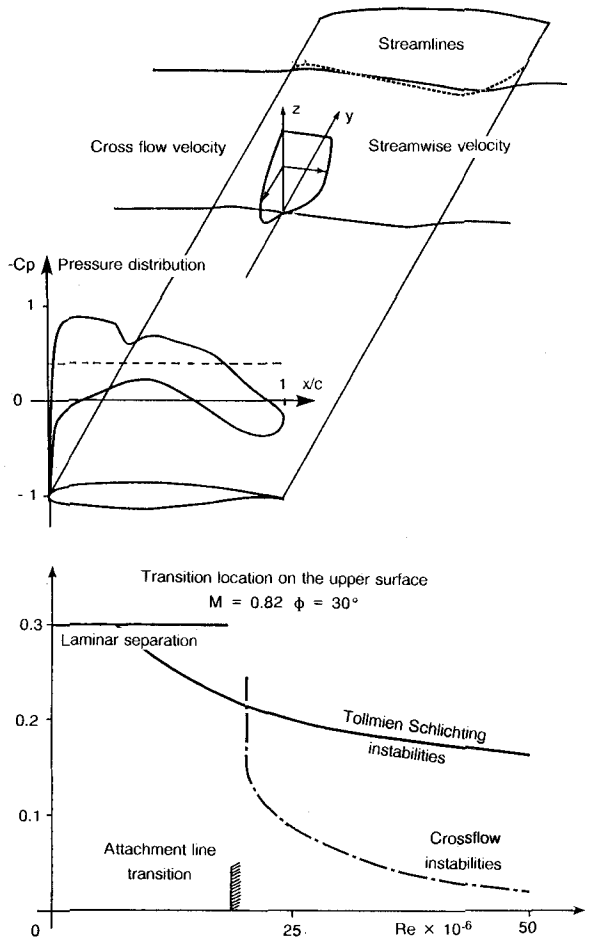

Fig. 2. Flow pattern and transition mechanisms on an infinite swept wing.

It is difficult to delimit the application of the natural laminar flow concept with accuracy because a large number of parameters (pressure distributions, sweep, Reynolds number, turbulence level) and different mechanisms of transition must be considered. However, NLF applications concern executive or short haul aircraft while HLFC applications concern mainly large transport aircraft. Since French aircraft manufacturers are concerned with the configurations mentioned above, research has been conducted in both of these fields.

2.1.1. Transition prediction tools

In order to design laminar flow configurations, accurate prediction methods have to be developed for the different transition mechanisms described in the previous section. These studies have been carried out by the ONERA/CERT DERAT department in Toulouse[6, 7]. The methods can be classified versus their degree of complexity as follows:

- empirical criteria;
- data base methods;
- stability computations.

The table presented in Figure 3 shows the various methods available at ONERA. Even if stability analysis codes give the amplification factor of the waves versus their frequencies, a limiting amplification factor still has to be specified to predict transition. This so-called N factor has to be calibrated versus experiment. These stability analysis codes need large computer time so simplified methods (empirical criteria and data base methods) are generally used for the purpose of designs for which many iterations are needed.

These simplified prediction methods are included in the various computer codes[8, 9] which have been used for the applications presented in the following sections. The laminar wing design procedure involves two- and three-dimensional methods which are summarized in Figure 4. The design begins with the definition of a basic airfoil, which results from a parametric study of pressure distributions and is obtained using direct and inverse methods as well as numerical optimization methods. The three-dimensional geometry of the wing is defined starting from the basic airfoil which generates the external wing. The optimization of the wing twist and generating airfoils is achieved by direct methods as well as numerical optimization.

	Empirical criteria	Data base methods	Stability computations
Tollmien-Schlichting instabilities	×	×	×
Crossflow ir.stabilities	×	under development	×
Attachment line transition	×		

Fig. 3. Transition prediction tools available at ONERA for compressible flows.

Configurations	Design methods	Configurations	Analysis methods
Airfoils	Numerical optimization / inverse	Airfoils	Full potential with weak and strong coupling / Navier-Stokes
Wings	Numerical optimization	Wings	Full potential with weak coupling
Nacelles		Nacelles	Full potential

Fig. 4. ONERA tools for transport aircraft studies.

2.1.2. Natural laminar flow

The ONERA experience on sailplanes (Figure 5) has been extended to the design of transonic laminar airfoils and wings for transport aircraft. Two examples are presented:

- Horizontal tail for an executive aircraft

The objective of these studies conducted in close collaboration with the AMD-BA company was to design a horizontal tail for an executive aircraft. The aim was to obtain laminar flow on at least 50% of the total surface (lower and upper) at cruise, i.e., $M = 0.80$, $C_L = 0.55, Re = 3.7 \times 10^6$.

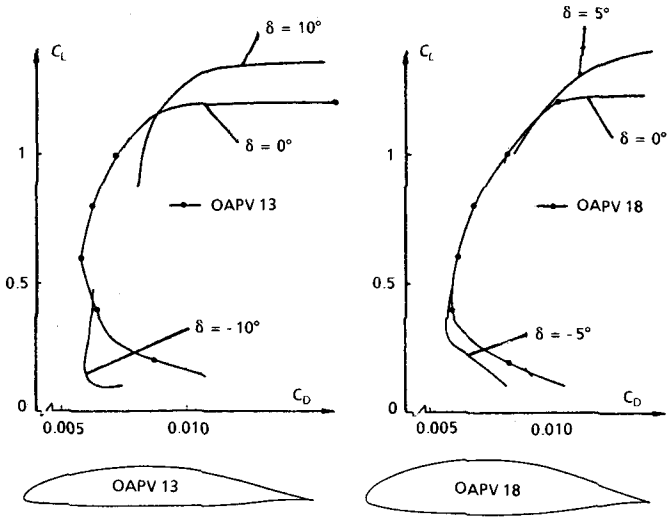

Fig. 5. Performances of ONERA airfoils for sailplanes. $V = 40$ m/s; $Re = 1.1 \times 10^6$.

The off-design constraints are related to the buffet onset margins, even in case of loss of the laminar flow, and to the low speed performance.

The planform of the horizontal tail has an aspect ratio of 4 and a taper ratio of 0.4. The sweep angle has been optimized to avoid unacceptable forward transition locations at cruise due to crossflow instabilities and to provide the required margin against buffeting.

In a second step, the generating airfoils and the twist distribution have been optimized taking into account the cruise condition (transition locations and lift-induced drag) and the low speed performance ($C_{L\,max}$).

In order to check the predictions, a 1/3 scaled model of the horizontal tail giving the flight Reynolds number has been tested in the S2MA pressurized transonic wind tunnel of the ONERA center at Modane.

The model was fitted with three sections of pressure holes and it was built for transition visualizations by infrared thermography. Furthermore, it was mounted on a side wall balance for total force and moment measurements.

Figure 6 presents a comparison between the predicted and the measured pressure distributions and transition locations in three sections. The good agreement shows that the above-described methods are reliable.

Turbulence measurements taken during the actual testing showed a turbulence level lower than 0.1%. This demonstrates that the flow quality in the wind tunnel is good enough to allow the experimental study of laminar configurations.

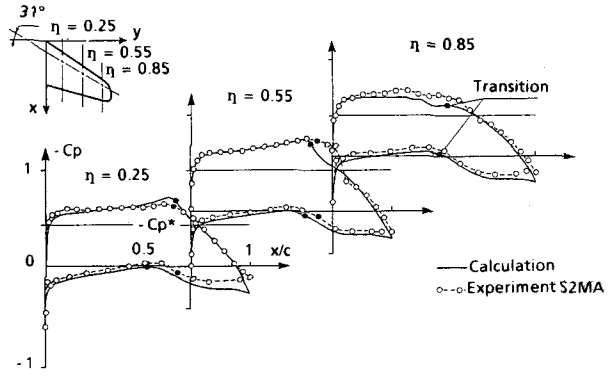

Fig. 6. Computed and measured pressure distributions on the horizontal tail. $M = 0.80$; $\alpha = 7.22°$; $Re = 3.7 \times 10^6$.

For the mid-span section the transition location given by infrared cameras[10] is plotted in Figure 7 versus the lift coefficient in the cruise conditions. For the cruise lift level, transition is due to a laminar separation which lies behind mid-chord. Increasing the lift coefficient decreases the negative pressure gradient on the upper surface and increases the negative pressure gradient on the lower side. Thus the transition location moves forward on both sides due to Tollmien-Schlichting instabilities on the upper surface and to crossflow instabilities on the lower surface. The same phenomena occur at low lift levels with an inversion of the instability type on the upper and the lower surfaces.

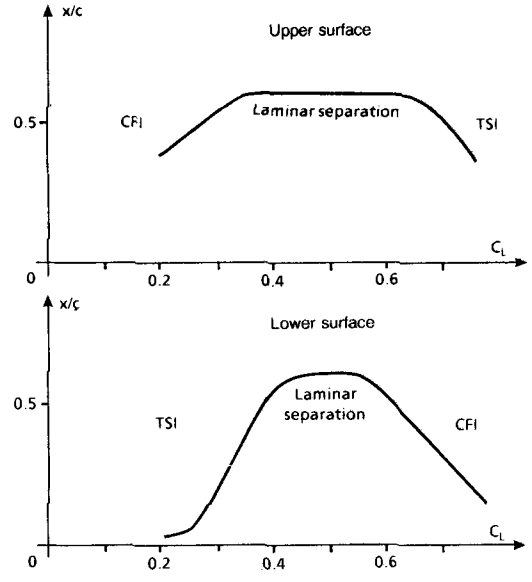

Fig. 7. Transition locations visualized by infrared thermography versus the lift coefficient at mid-span. $M = 0.80$; $Re = 3.7 \times 10^6$.

Tests with a fixed transition at 7% of the chord on both sides have been made. By removing the lift-induced drag component of the total drag, these tests make it possible to estimate the skin friction drag reduction of the laminar horizontal tail over a turbulent configuration. This gain is plotted in Figure 8 in a C_L versus Mach number diagram. It can be seen from the figure that for the design conditions, a 50% gain has been achieved. This gain was obtained without penalty to the off-design conditions. No separation occurs on the horizontal tail when transition is fixed at the leading edge.

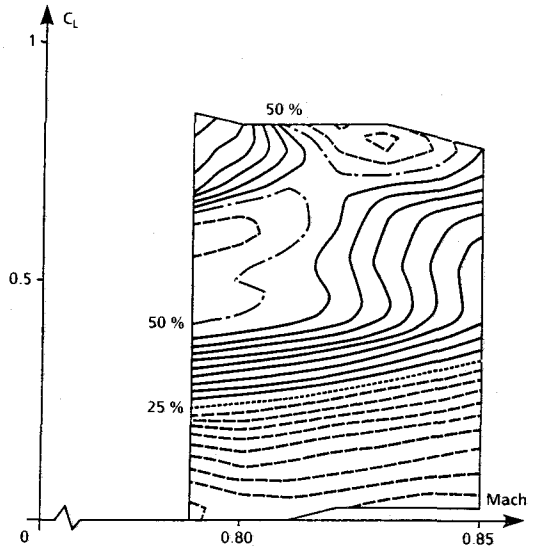

Fig. 8. Skin friction drag reduction obtained with the laminar horizontal tail.

- Natural laminar flow wing

The second example of natural laminar flow applications, which was developed in cooperation with Aerospatiale, concerns a wing for a short-haul aircraft. The planform of the wing has an aspect ratio of 10, a taper ratio of 0.33 and a quarter chord sweep angle of 12°.

The design was made in the following cruise conditions: $M = 0.74$, $0.36 < C_L < 0.50$, $Re = 22 \times 10^6$. A second design point, typical of the climb conditions, has also been taken into account $M = 0.55$, $C_L = 0.45$, $Re = 19 \times 10^6$.

The computed pressure distributions of the optimized wing are plotted in Figure 9 for the cruise conditions. The corresponding transition locations are at about 60% of the chord on both sides giving again 50% skin friction drag reduction compared to a fully turbulent design. This gain transposed to the complete aircraft gives a total drag reduction of 10%.

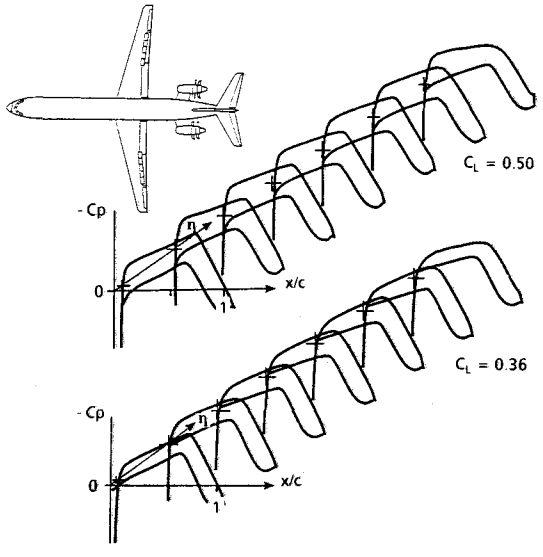

Fig. 9. Computed pressure distributions on the wing of a short haul aircraft. $M = 0.74$; $Re = 22 \times 10^6$.

For the climb conditions, the transition is located at 15% of the chord on the upper surface and 60% of the chord on the lower surface giving a skin friction drag reduction of 25% over a fully turbulent design. Since it is not possible in Europe to achieve the design Reynolds number in the existing wind tunnels on a 3D model, a swept wall-to-wall model has been built and tested in the T2 transonic cryogenic wind tunnel of the ONERA CERT/DERAT department in Toulouse.

The model was designed so as to obtain the same pressure distribution at mid-span as on the wing. With a mid-span chord of 0.186 m, Reynolds numbers up to 20×10^6 can be obtained.

Figure 10 shows the wall-to-wall swept model planform and the corresponding computed pressure distributions for the cruise conditions. It can be seen from the figure that the three-dimensional effects are very small.

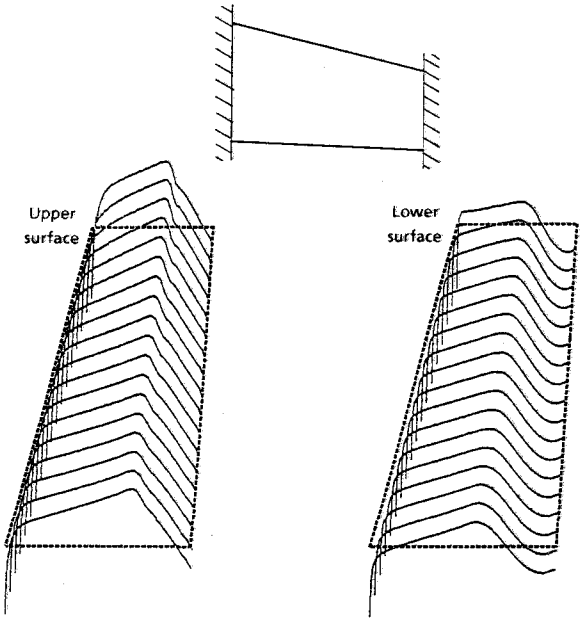

Fig. 10. Computed pressure distribution on the wall-to-wall swept model. $M = 0.74$; $Re = 20 \times 10^6$.

Figure 11 shows the measured drag polars of the mid-span section in cruise conditions. To avoid possible problems at low temperatures, free transition tests have been performed for Reynolds numbers up to 11.5×10^6. A large decrease of the drag is demonstrated in free transition compared to the results in fixed transition at 7% of the chord. Since with fixed transition there is no separation, it is clear that the drag is very small due to a transition location measured by thermocouples at 60% of the chord on the upper surface and 55% of the chord on the lower surface.

These two wing designs show that large drag benefits can be achieved with the natural laminar flow technology.

It can be pointed out that even in the case of loss of laminar flow, the NLF design exhibits good characteristics. However, natural laminar wings have two disadvantages:

- the margin between the cruise Mach number and the drag rise Mach number is smaller than for a turbulent

design (although usual buffet margins are satisfied);
- conventional leading edge slats cannot be used on a NLF wing in low speed conditions.

Increasing the Reynolds number or the sweep angle of the wing will reduce the extent of natural laminar flow. These limits have been plotted in Figure 12 in a Reynolds number and sweep angle diagram. Iso-transition location lines are computed assuming infinite swept wing conditions.

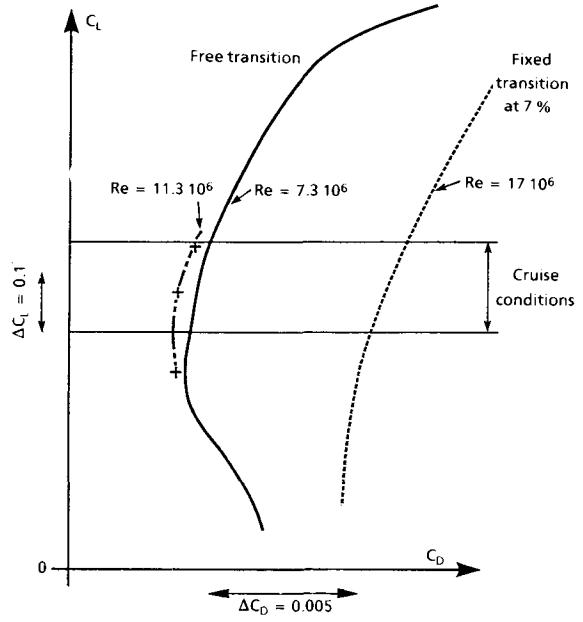

Fig. 11. Measured drag in the mid-span section at M=0.74.

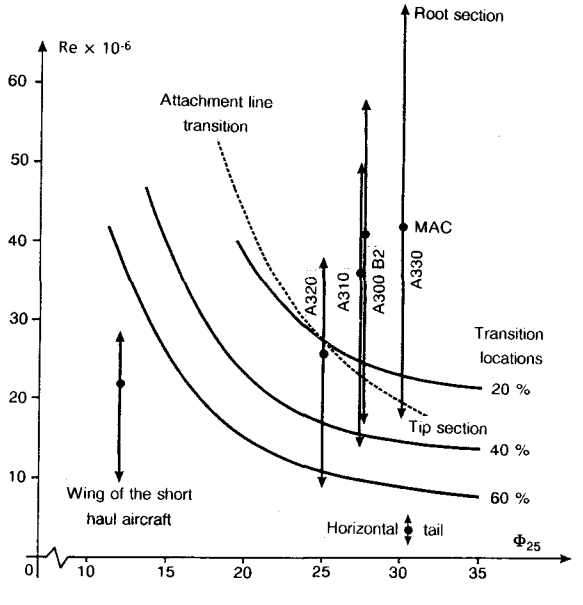

Fig. 12. Limits of the natural laminar flow concept. Infinite swept wing computations.

The two NLF designs presented previously lie within 60% of the chord transition location line. For the Airbus transport aircraft wings (represented by vertical lines), it can be shown that a large part of laminar flow cannot be obtained with the NLF concept. Moreover, the attachment line transition limit has to be taken into account for all these aircraft. In these conditions, laminar flow can only be obtained through suction of the boundary layer.

2.1.3. Hybrid laminar flow control

Since the most promising solution for laminar flow control seems to be the application of suction in the leading edge region ahead of the wing front spar, this is the concept which has been investigated at ONERA.

Three applications of hybrid laminar flow control will be described. They concern different components of a large transport aircraft: the wing, the fin and the nacelles.

- HLFC wing

The study was oriented toward the comparison between a laminar wing and a turbulent one for a long range transport aircraft. The main wing characteristics are:

- surface 350 m^2
- aspect ratio 9
- quarter chord sweep angle $27.5° \leq \phi \leq 30°$
- thickness to chord ratio of 15% at the root and 10.5% at the tip
- suction to be applied ahead of the front spar up to 20% of the chord for the laminar wing.

The design conditions are: $M = 0.82$, $C_L = 0.44$, $Re = 42 \times 10^6$,

The turbulent wing was designed for a 30° sweep angle using a basic airfoil developed at ONERA. For the laminar wing, the best results were obtained in terms of transition location versus transonic performance with a 27.5° sweep angle: this small reduction allows a significant increase of the laminar flow extent without increasing the wave drag at cruise.

Five generating airfoils and the twist distribution were defined so as to obtain the same pressure gradients over the span as with the basic airfoil optimized in infinite swept wing conditions.

Figure 13 shows the planforms of the two wings and their computed pressure distributions in cruise conditions. The negative pressure gradients were maintained up to 60% of the chord on the upper surface and up to 55% of the chord on the lower surface.

Assuming suction between 0% and 20% of the chord on both sides, transition location was computed for different suction distributions and different mass flow rates. From this parametric study, it appears that a linear suction distribution with a mean suction velocity of 0.1 m/s gives the best results in terms of transition locations versus suction rates. For this suction velocity distribution, transition locations on the laminar wing, computed while taking into account Tollmien-Schlichting and crossflow instabilities, are drawn in Figure 14. Due to the wing taper, transition location ranges from 30 per cent of the chord at the root up to 50 per cent of the chord at the tip on the upper surface. On the lower surface, the results are about the same with, however, some shift of the transition location towards the leading edge between 15% and 30% of the span. This could be improved by a slight wing shape modification in that region.

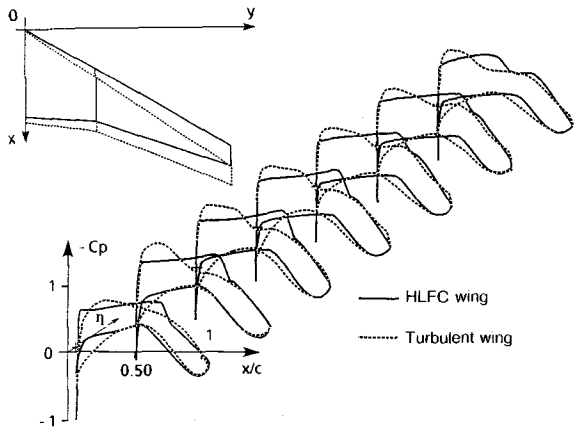

Fig. 13. Computed pressure distributions on the HLFC and the turbulent wing. $M=0.82$; $C_L=0.435$; $Re=42 \times 10^6$.

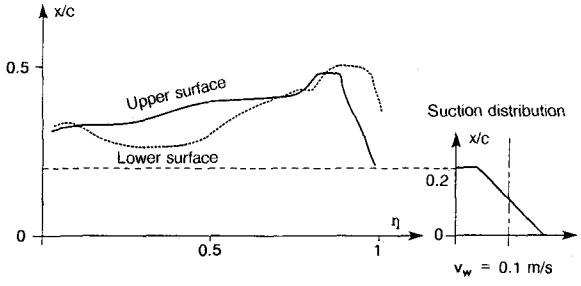

Fig. 14. Computed transition locations on the HLFC wing. $M=0.82$; $C_L=0.435$; $Re=42 \times 10^6$.

For the turbulent wing, as well as for the laminar wing without suction, transition is located at the leading edge.

The viscous drag of the laminar wing is 35% lower than that of the turbulent wing which gives a total aircraft drag reduction of 8% for the cruise conditions. This is obtained with a suction mass flow rate of 3.7 kg/s. The achieved drag reduction could be improved by further work on the wing design and on the suction distribution. We thus think that a 10% drag reduction for the same mass flow rates constitutes a realistic estimate. This is smaller than other figures published in the literature which to us seem too optimistic at least for the type of aircraft involved in our study.

The power of the suction system was estimated under the following assumptions:

- a pressure difference of $\Delta C_p = 0.2$ is applied between the wing surface and the suction chamber;
- the sucked flow is ejected under the free-stream conditions;
- the suction system efficiency is 0.85.

This gives a power of 266 kW for the suction system. Taking into account this power, the fuel consumption reduction which seems achievable is 9% for the aircraft. It is underlined that the laminarization of the upper surface alone will give a 6% fuel consumption reduction which is still very large and will allow the use of a high lift leading edge system like a Krüger flap.

The computations carried out on the laminar wing with fixed transition at the leading edge show that in the case of suction system failure, there is no separation.

Large drag benefits can thus be achieved with HLFC wings for large transport aircraft.

When looking at the application of the HLFC concept on existing Airbus type aircraft, it appears that under operational conditions the fin offers great advantages for experimentation with this new technology. There is no deicing or high lift systems which leaves a room in the leading edge region to install the suction ducts.

So an aerodynamic study has been carried out in cooperation with Airbus Industrie to estimate what benefit in terms of transition locations and aircraft drag reduction might be expected.

- HLFC fin

The A320 fin planform chosen for the study has a quarter chord sweep angle of 35°. For the cruise Mach number (M = 0.78), the Reynolds number based on the mean aerodynamic chord is 24×10^6.

As for the wing, three-dimensional transonic viscous flow computations were carried out to predict the transition locations. Analysis was performed on the original fin and an optimized fin was designed to obtain a better compromise between the transition location and the suction flow rate.

The three-dimensional effects appear to be very small and Figure 15 shows the pressure distributions at mid-span on the actual fin and on the optimized fin. Suction has been applied up to 20% of the chord, ahead of the front spar.

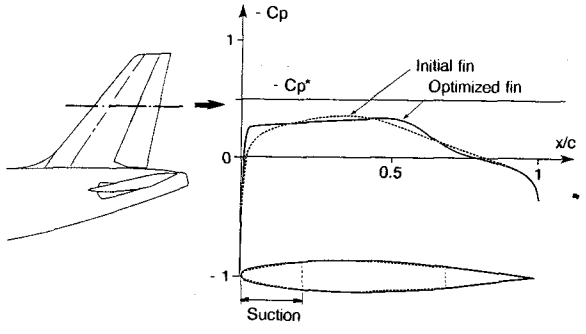

Fig. 15. Computed pressure distributions at mid-span on the A320 fin. $M=0.78$; $Re=24 \times 10^6$.

The transition locations at mid-span are plotted in Figure 16 versus the mean suction velocity for both fins, taking into account the Tollmien-Schlichting and crossflow instabilities.

Without suction the transition is located very near the leading edge due to crossflow instabilities.

The modified fin gives a pressure distribution which prevents the development of the crossflow instabilities in the first 10% of the chord and which allows a reduction of the suction rate necessary for maintaining a laminar flow. With the suction velocity distribution shown in Figure 16 and a mean velocity value of 0.15 m/s, transition is located at 31% of the chord with the original fin and at 42% of the chord with the modified one.

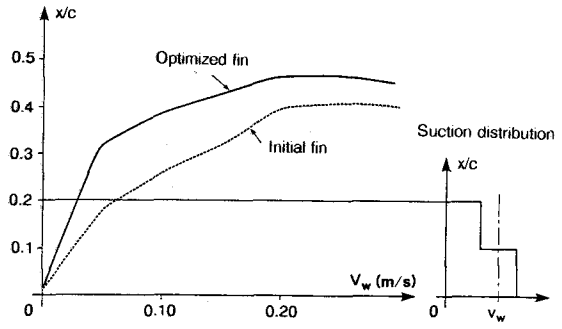

Fig. 16. Computed transition locations at mid-span on the A320 fin. $M=0.78$; $Re=24 \times 10^6$.

This gives for the fin a total drag reduction of respectively 36% and 44%, for a suction mass flow rate of 0.41 kg/s. Using the assumption presented in the previous section, the suction power has been estimated at 23 kW. Taking this power into account, the fuel consumption reduction is 1.1% with the original fin and 1.5% with the new one.

These figures are significant and it appears that the A320 fin should be a good support for a wind tunnel-flight test program aiming at the development of the HLFC technology.

- HLFC nacelles

The last aircraft component for which the feasibility of laminarization by boundary layer control has been studied is the nacelle.

Several types of nacelles representative of those used on Airbus aircraft have been considered, but only results concerning a long duct nacelle are presented.

The shape of this nacelle is shown in Figure 17 with the pressure distributions computed for the following conditions: $M = 0.76$, an inlet mass flow rate of 0.68, and a Reynolds number of 30×10^6. From the figure, it can be seen that for the upper and the lateral parts of the nacelle, leading edge expansion peaks are present as well as a pressure recovery located around 20% of the chord for all the sections.

The suction area has been chosen taking into account practical constraints like the access doors and the pylon locations.

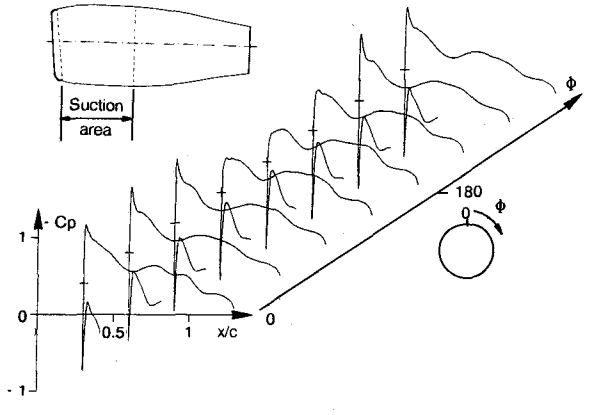

Fig. 17. Computed pressure distributions on a long duct nacelle. $M=0.76$; $\varepsilon=0.68$; $Re=30 \times 10^6$.

Figure 18 shows the computed transition locations. Without suction, transition is located near the leading edge between $\phi=0°$ and $\phi=130°$ as well as between $\phi=230°$ and 360°. On the lower side, transition occurs at around 12% of the chord.

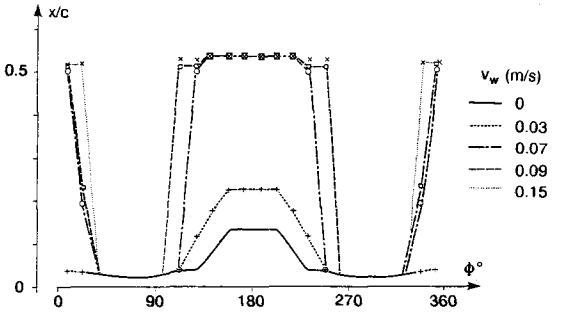

Fig. 18. Computed transition locations on a long duct nacelle. $M=0.76$; $\varepsilon=0.68$; $Re=30 \times 10^6$.

Applying suction between 3% and 40% of the nacelle length, transition moves backward mainly on the lower side. With a constant suction velocity of 0.09 m/s, transition is located up to 50% of the chord between $\phi=110°$ and $\phi=250°$.

If suction starts at 2% of the chord instead of 3%, the extent of the laminar flow covers 52% of the wetted area of the nacelle ($S_W=29.7$ m^2) for the same suction velocity. In such conditions, the drag reduction for the nacelle is about 37% and the suction mass flow needed is 0.4 kg/s. This allows us to estimate a 1% total drag reduction for an A320 type aircraft.

It appears from this study that the actual shapes of the nacelles are not adapted to laminar flow and that with new designs, greater benefits could be obtained.

These examples show that applying laminar boundary layer control to the various components of a large transport aircraft gives significant drag reduction. Estimates of the drag reduction and the fuel consumption reduction for a 150 pax medium range aircraft and a 300 pax long range aircraft are summarized in Figure 19.

	150 pax medium range aircraft		300 pax long range aircraft	
	Drag reduction	Fuel consumption reduction	Drag reduction	Fuel consumption reduction
Wing	11 %	10 %	10 %	9 %
Tail + fin	4 %	3.5 %	3.5 %	3 %
Nacelles	1.5 %	1 %	1.2 %	1 %
Total	16.5 %	14.5 %	14.7 %	13 %

Fig. 19. Expected drag reductions with HLFC technology compared to conventional turbulent designs.

Applying the suction to the wing, the horizontal tail, the fin and the nacelles, the fuel consumption reduction approaches 15%. These figures should encourage the aircraft manufacturers and the airline companies to support research programs aiming at the development of this new technology.

2.1.4. Attachment line transition

To complete the chapter devoted to ONERA research on laminar flows, the activity concerning the validation of transition prediction methods must be mentioned. The research is carried out in close collaboration by the Aerodynamics' department and the CERT/DERAT department. It concerns the different mechanisms of transition (TSI, CFI and ALT) with and without suction.

The study of the ALT phenomenon, presented here as an example of this research, has been undertaken on a large variable swept-wing model in the pressurized low speed wind tunnel F1 of the ONERA center at Le Fauga-Mauzac.

The rectangular wing has a chord of 0.5 m normal to the leading edge, a variable sweep between 0° and 40° and the span of the model is 2 m for the highest sweep angle.

Transition is detected by hot films which are located near the attachment line all along the span.

Figure 20 shows the response of the hot films when increasing the wind tunnel velocity in the following conditions: $\Phi = 40°$, $\alpha = 10°$, $p_t = 1$ bar.

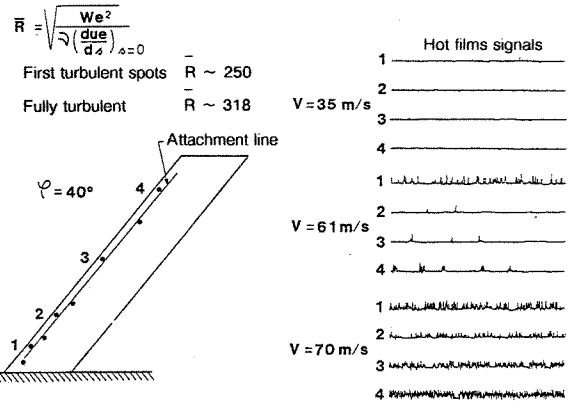

Fig. 20. Validation of the attachment line transition criterion in incompressible flow. $\alpha = 10°$; $P_t = 1$ bar.

For the lowest velocity ($V = 35$ m/s), the attachment line remains laminar. At 61 m/s ,turbulent spots coming from the wind tunnel floor boundary layer are convected along the attachment line. Increasing the velocity up to 70 m/s leads to a fully turbulent attachment line as shown by the hot film signals.

This experiment, described in detail[11], makes it possible to validate the attachment line criterion based on the Reynolds number $\bar{R}$ in incompressible flow. The first turbulent fluctuations are detected for $\bar{R} \sim 250$ and the attachment line is fully turbulent for $\bar{R} \sim 318$.

Figure 21 shows that a suction applied on the wind tunnel floor near the leading edge of the wing delays the attachment line transition at higher Reynolds numbers.

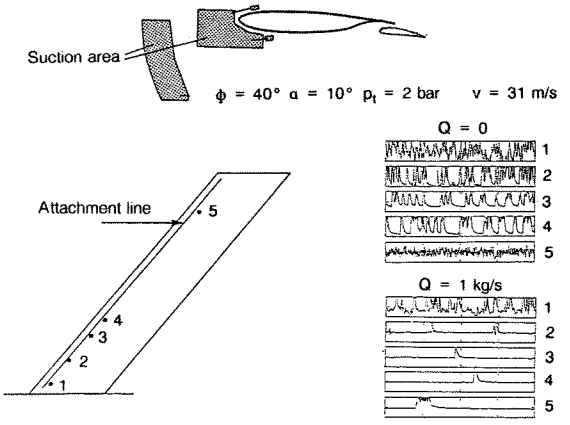

Fig. 21. Effect of wall suction on the attachment line transition.

2.2. Turbulent flow

The second skin friction drag reduction technology which is currently receiving the greatest attention is the use of turbulent boundary layer manipulators. Among the various devices[12] which can be used the riblets seem to be the easiest to apply to an aircraft.

ONERA has undertaken a large research program in order to validate this approach. This has been done in close cooperation with Aerospatiale and Airbus Industrie. The major steps of this research program have been:

- experiments on flat plates at low speed including yaw effect;
- experiments on a body of revolution at transonic speed including yaw effect;
- experiments on airfoils at subsonic and transonic speeds;
- experiments on an A320 model in the S1MA wind tunnel.

The first three steps have been conducted by the CERT/DERAT department[13, 14]. Results of these studies having been promising, the investigations have been pursued on a large transport aircraft model in the S1MA wind tunnel.

Using the results of the previous investigations and viscous flow computations on the A320 configuration, the V groove shape ($s = h$) has been chosen, the size leading to a h_W^+ of about 8 in cruise conditions.

The riblet film was provided and installed on the model by the 3 M France company. Two thirds of the model surface were covered. Figure 22 shows the A320 model in the wind tunnel.

The drag reduction obtained with riblets for two Mach numbers is plotted in Figure 23. It can be noticed from the figure that the highest drag reduction has been measured at $M = 0.7$.

For the cruise lift level 1.6% drag reduction has been obtained. Considering these results as significant Airbus Industrie decided to perform a riblet flight test on an A320 aircraft. The flight tests carried out in 1989 have confirmed the prediction based on the wind tunnel results.

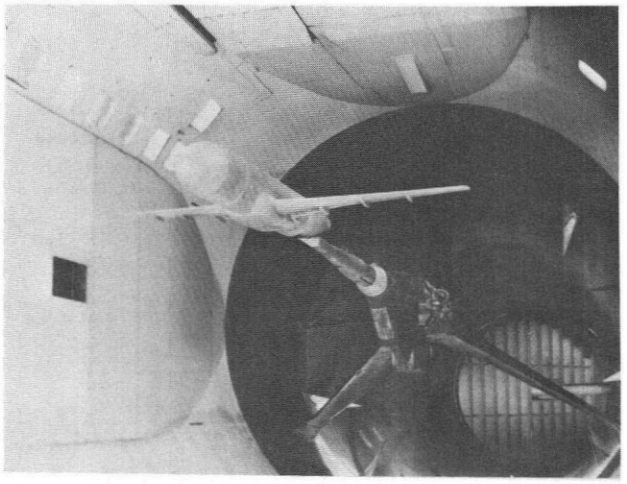

Fig. 22. Riblet test on an A320 model (scale 1:11) in the S1MA wind tunnel.

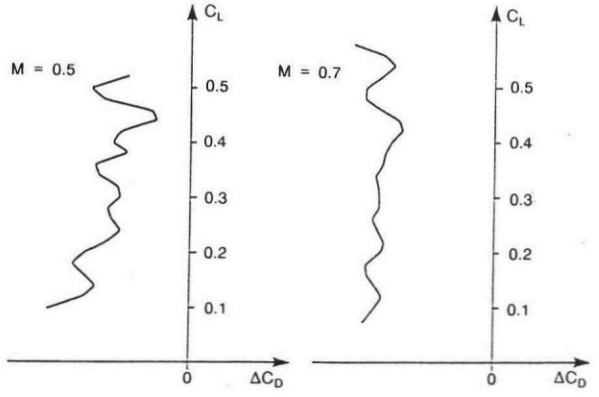

Fig. 23. Drag reduction obtained with riblets on the wing body configuration in S1MA.

3. Drag due to lift reduction

The second major drag component as shown in Figure 1 is the lift induced drag. To reduce this term, wings of larger aspect ratio could be used but this would lead to a weight penalty that might offset the drag reduction.

Since optimal wing aspect ratio for a transport aircraft is a compromise between the weight, the sweep angle and the wing thickness, it is clear that for a given level of technology there is not a great possibility of increasing wing aspect ratios.

Moreover, modern commercial aircraft wings have very good aerodynamic efficiency which means that potential benefits for reducing the drag due to lift are not very large for the actual aircraft configurations.

However, wing tip devices like winglets and wing tip sails can produce some gain by increasing the effective span of the wing and recovering some of the energy from the tip vortices.

These two objectives can be met with the wing tip turbine concept. Mounting a turbine in the tip vortices will make it possible to extract energy[15] which can be used to produce electric power through a generator, and to supply the main electric power in case of failure. When no electric power is needed, the turbine can be stopped and it then becomes a wing tip device.

In a large cooperative program conducted by Aerospatiale, this concept has been checked at low speed on an A320 half model in the CEAT S5 wind tunnel in Toulouse. Detailed flowfield measurements of the wing tip vortex by means of a 5 hole pressure probe have first been performed on the actual wing in order to determine the three velocity components.

Using these data, a four blade turbine has been designed with three-dimensional Euler and boundary layer codes. Since the blade Reynolds number is very low in the test configuration, much attention has been paid to the blade design to avoid separation. The turbine shape as well as the computed isobar-lines are shown in Figure 24. The turbine has been installed on the model and tests were performed for both free and fixed turbine configurations.

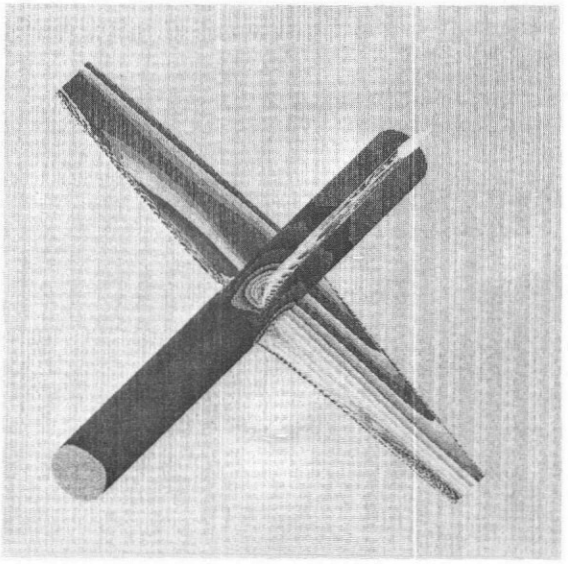

Fig. 24. Isobar-lines on the wing tip turbine computed by an Euler method.

For the fixed turbine configuration (Figure 25), the flow field measurement behind the turbine exhibits a large reduction of the tangential components of the velocity compared to the flowfield of the basic configuration. In addition, a 6% lift induced drag reduction has been obtained from the balance measurements for the cruise lift condition.

For the free turbine configuration, the power developed on the turbine shaft versus the r.p.m. is plotted in Figure 26. Extrapolation to full-scale in cruise conditions shows that this will give a power of about 44 kW for two turbines which is higher than the emergency power required on the actual aircraft.

4. Shock boundary layer interaction

Since the optimum aerodynamic efficiency of a wing ($M \times C_L/C_D$) is obtained in transonic flow with a weak shock wave, increasing the Mach number at fixed C_L or C_L at fixed Mach number increases the strength of the shock and the wave drag. Margins between the optimum design conditions and buffet or drag rise boundaries can be improved if the shock boundary layer interaction is controlled in order to avoid separations.

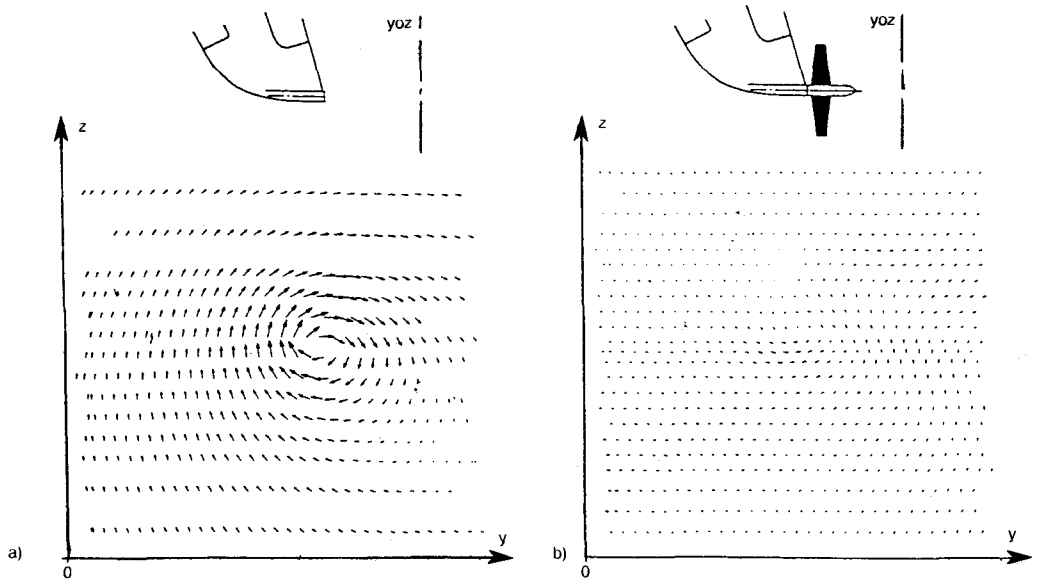

Fig. 25. Influence of the wing tip turbine on the tip vortex. Tangential flow components. a) without turbine, b) with the fixed turbine.

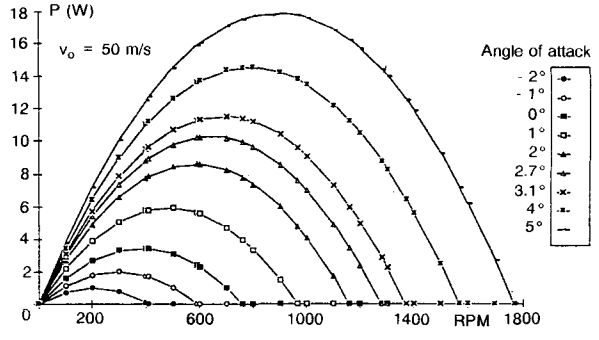

Fig. 26. Shaft power recovered by the wing tip turbine on an A320 half model (scale 1:7.6) in the S5 wind tunnel of the CEAT test center.

Among the different control systems which have already been investigated, the passive shock boundary layer control[16] is the most interesting since no additional energy is needed. This concept is presented in Figure 27. The basic idea is to place a perforated surface with a cavity underneath it at the shock location.

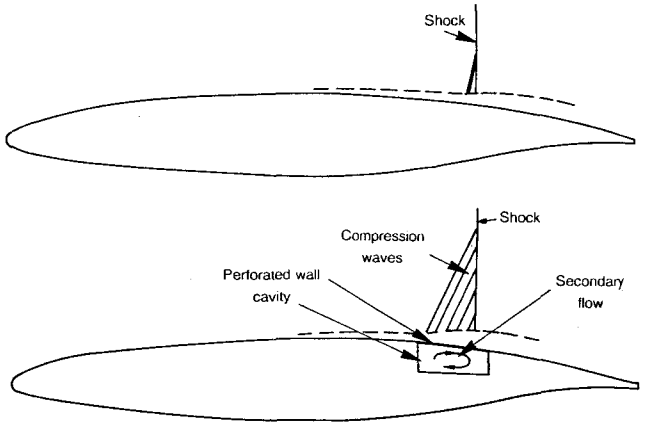

Fig. 27. Schematic flow pattern due to the passive shock boundary layer control system.

Due to the pressure jump across the shock a secondary flow is initiated in the cavity. The blowing upstream to the shock transforms the straight shock into a lambda shock configuration and its strength is reduced by the presence of the compression waves.

On the other hand, the blowing increases the boundary layer thickness ahead of the shock and the perforated wall induces a rugosity effect. This gives an increase of the viscous drag which may balance the decrease of the wave drag.

This concept seems particularly well-adapted to laminar airfoils for the following reasons:

- rearward shock location behind the rear spar;
- shock location not too sensitive to the Mach number or to the lift coefficient;
- lower margins between cruise conditions and buffet or drag rise boundaries compared to conventional airfoils.

This concept has been tested on a laminar airfoil in the T2 wind tunnel. Several preforated surfaces with different hole diameters and porosity factors have been investigated.

Figure 28 shows the measured pressure distribution on the tested laminar airfoil as well as the total pressure distribution in the wake for the conditions $M=0.77$, $\alpha=0.5°$ ($C_L \sim 0.45$). The results are presented for the solid surface airfoil and for the airfoil fitted with two different cavities of 10% chord length. The porosity factors of the perforated surface are 3.5% (A) and 8% (B) for the same hole diameter.

The transition is fixed at 50% of the chord on the upper surface to avoid a laminar boundary layer shock interaction.

With both cavities, the shock strength is clearly reduced and spread over the width of the perforated surface. The corresponding benefit is seen on the wake total pressure distribution. Highest benefit effects are obtained with the porosity factor of 8%.

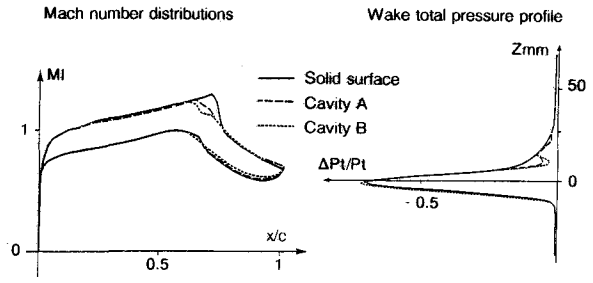

Fig. 28. Effects of passive shock boundary layer control on a laminar airfoil. $M=0.77$; $\alpha=0.5°$.

Unsteady pressure measurements near the trailing edge of the airfoil show a decrease of the RMS pressure level which confirms the favourable effect of the passive control on the shock strength.

However, no significant total drag reductions have been obtained which means that the increase of the viscous drag offsets the decrease of the wave drag. Additional theoretical and experimental studies must be undertaken in order to optimize this concept.

5. Problems associated with the introduction of new technologies

As has been demonstrated in the previous chapters, some of the new technologies which have been investigated at ONERA these last years appear promising. However, a lot of problems have to be solved which demands close cooperation between Aerodynamics and other disciplines. Some of them are listed below:

– Laminar flow:

- validation of the transition prediction methods with and without suction at high Reynolds numbers ($Re > 10 \times 10^6$) in wind tunnel and in flight;
- measurements of turbulence level in wind tunnel and in flight;
- study of rugosity effects and of manufacture tolerance;
- study of a solution to delay attachment line transition (suction, local shape modification);
- development of the technology and the manufacturing techniques for the suction system (HLFC);
- study of the influence of the hole diameters and porosity factor for the suction surface (HLFC);
- investigation of the possible high lift systems to be used on a laminar wing.

– Riblets:

- study of the operational aspects.

– Wing tip turbine:

- demonstration of the efficiency at transonic speed and realistic scale.

– Shock boundary layer control:

- numerical tools as well as detailed flow analysis are needed in order to better understand and to optimize the concept;
- demonstration on a three-dimensional configuration.

Since the development of this new technology will require a great effort and will be very expensive, cooperations are necessary.

The BRITE-EURAM Aeronautical program, launched recently and sponsored by the Economic European Community, constitutes a valuable step in that direction.

6. Conclusion

During these last few years, ONERA activities on drag reduction have been oriented towards the investigation of the potential benefits which can be expected by applying certain new technologies.

The different concepts which have been studied are:
- natural laminar flow;
- hybrid laminar flow control;
- riblets;
- wing tip turbine;
- shock wave boundary layer control.

For each of these topics, both theoretical and experimental studies have been carried out which demonstrate the potential and also the limits of these concepts. These preliminary studies have also shown that a lot of work is still needed in order to allow manufacturers to design aircraft using these new technologies.

The paper presents results from studies which have been supported by the French government agencies (DGAC, STPA), Aerospatiale and AMD-BA companies and Airbus Industrie.

References

1. CAMPBELL R.L., WAGGONER E.G., PHILLIPS P.S.: "Design of a Natural Laminar Flow Wing for a Transonic Corporate Transport". AIAA-86-0314, Reno, 1986.

2. REDEKER G., HORSTMANN K.H., KÖSTER H., QUAST A.: "Investigations on High Reynolds number Laminar Flow Airfoils". ICAS-86-113, 1986.

3. PFENNINGER W.: "Laminar Flow Control Laminarization". AGARD-R-654, pp. 3-1 to 3-75, 1977.

4. "Hybrid Laminar FLow Control Study". Final Technical Report (Boeing). NASA CR 165930, 1982.

5. FISCHER M.C., WRIGHT A.S., WAGNER R.D.: "A Flight Test of Laminar FLow Control Leading-Edge Systems". NASA TM 85712, 1983.

6. ARNAL D., HABIBALLAH M., COUSTOLS E.: "Laminar Instability Theory and Transition Criteria in Two and Three-Dimensional Flow". La Recherche Aérospatiale, No 1984-2, 1984.

7. ARNAL D.: "Transition Prediction in Transonic Flow". IUTAM Symposium Transsonicum III, Göttingen, 1988.

8. LE BALLEUR J.C.: "Strong Matching Method for Computing Transonic Viscous Flows Including Wakes and Separations. Lifting Airfoils. La Recherche Aérospatiale, No 1981-3, 1981.

9. LE BALLEUR J.C., LAZAREFF M.: "Computation of Three-Dimensional Viscous Flows on Transonic Wings via Boundary Layer Inviscid Flow Interaction". La Recherche Aérospatiale, No 1983-3, 1983.

10. GAUFFRE G.: "Detection of Laminar-Turbulent Transition by Infrared Thermography". La Recherche Aérospatiale, No 1988-2, 1988.

11. ARNAL D., JUILLEN J.C.: "Etude de la transition et de la contamination de bord d'attaque sur ailes en flèche". AGARD/FDP, Cesme, 1988.

12. WILKINSON S.P., ANDERS J.B., LAZOS B.S., BUSHNELL D.M.". Turbulent Drag Research at NASA Langley - Progress and Plans". Int. Conf. on Turbulent Drag Reduction by Passive Means, London, 1987.

13. COUSTOLS E., COUSTEIX J.: "Turbulent Boundary Layer Manipulation in Zero Pressure Gradient". 16th ICAS Congress, Jerusalem, 1988.

14. COUSTOLS E.: "Behaviour of Internal Manipulators - Riblet Models in Subsonic and Transonic Flows". AIAA 2nd Shear Flow Conference, Tempe, 1989.

15. PATTERSON Jr. J.C., FLECHNER S.G.: "Exploratory Wind Tunnel Investigation of a Wing-tip Mounted Vortex Turbine for Vortex Energy Recovery". NASA TP 2468, 1985.

16. STANEWSKY E., KROGMANN P.: 'Transonic Drag Rise and Drag Reduction by Active/Passive Boundary Layer Control". AGARD-R-723, pp. 11-1 to 11-41, 1985.